Journal of Nanotechnology

WILEY

RESEARCH ARTICLE OPEN ACCESS

Equisetum diffusum–Mediated Synthesis of Cobalt Oxide Nanoparticles for Multifaceted Biomedical Applications

Nasir Assad[1] | Tehreem Riaz[1,2] | Muhammad Naeem-ul-Hassan[1] | Muhammad Fayyaz Ur Rehman[1] | Marzia Batool Laila[1] | Muhammad Nauman Khan[3,4] | Ahmed Vandy[5] | Iram Zahra[1] | Sharia Fatima[1] | Barkat Ullah[4]

[1]Institute of Chemistry, University of Sargodha, Sargodha 40100, Pakistan | [2]School of Chemistry, University of the Punjab, Quaid-i-Azam Campus, Lahore 54590, Pakistan | [3]Department of Botany, University of Chakwal, Chakwal 48800, Punjab, Pakistan | [4]Department of Botany, Islamia College Peshawar, Peshawar 25120, Pakistan | [5]Faculty of Pharmaceutical Sciences, College of Medicine and Allied Health Sciences, University of Sierra Leone, Freetown, Sierra Leone

Correspondence: Ahmed Vandy (ahmedvandy@gmail.com)

Received: 7 December 2025 | **Revised:** 10 March 2026 | **Accepted:** 31 March 2026

Academic Editor: DHRUBA JYOTI MAJUMDAR

Keywords: antibacterial activity | antioxidant activity | cobalt oxide nanoparticles | green synthesis | hematological activities

ABSTRACT

The present study reports, for the first time, the green synthesis of cobalt oxide nanoparticles (Co_3O_4NPs) using aqueous extract of *Equisetum diffusum* as a natural reducing and stabilizing agent. The synthesized ED@Co_3O_4NPs were comprehensively characterized using various techniques: UV–Vis spectroscopy revealed an absorption peak at 323 nm; FTIR confirmed the presence of functional groups in the ED extract and ED@Co_3O_4NPs. XRD confirmed the formation of crystalline spinel-phase Co_3O_4 with an average crystallite size of 15.17 nm, whereas SEM analysis showed uniformly distributed spherical nanoparticles with an average diameter of 58.56 nm. DLS and zeta potential (−32 mV) indicated good colloidal stability. The biological potential of ED@Co_3O_4NPs was evaluated, demonstrating significant antibacterial activity against *Pseudomonas aeruginosa* (25 mm), *Escherichia coli* (22 mm), and *Staphylococcus epidermidis* (12 mm). Antioxidant assays revealed a concentration-dependent increase in activity, with DPPH scavenging percentages from 38.75% to 80.41% and FRAP reducing power from 26.05 (mg AAE/g) to 70.44 (mg AAE/g). Hemolytic activity ranged from 0.10% at (0.5 μg/μL) to 3.76% at (5 μg/μL), indicating low toxicity at lower concentrations. Preliminary anticoagulant and thrombolytic assays suggested a promising hemostatic modulation potential. These findings highlight the potential of ED@Co_3O_4NPs for various biomedical applications.

1 | Introduction

Nanotechnology has emerged as one of the most dynamic and rapidly expanding fields of scientific research worldwide [1]. Metal and metal oxide nanoparticles (NPs) synthesized through nanotechnological approaches are employed in several fields such as electrochemistry catalysis [2, 3], sensing [4, 5], pharmaceuticals, biomedicine [5], cosmetics [6], and food technology [7]. The biological and chemical characteristics of nanostructures are superior to those of bulk materials owing to their small size and high surface-to-volume ratio [8, 9].

Among the various metal and metal oxide NPs, cobalt oxide NPs (Co_3O_4NPs) have attracted considerable scientific interest owing to their versatile applications in several fields, including biomedicine [10]. Several approaches have been used to synthesize Co_3O_4NP; however, conventional physicochemical methods are often energy-intensive, time-consuming, costly, and environmentally hazardous [11]. To overcome these challenges, a biosynthesis approach is employed, using plant extracts and other renewable and sustainable biological resources as natural reducing and stabilizing agents [12, 13]. These methods require less heat energy, fewer chemical additives, are inexpensive, and most

This is an open access article under the terms of the Creative Commons Attribution License, which permits use, distribution and reproduction in any medium, provided the original work is properly cited.

Copyright © 2026 Nasir Assad et al. *Journal of Nanotechnology* published by John Wiley & Sons Ltd.

significantly, are nontoxic and environmentally friendly [14]. Moreover, bioactive phytoconstituents such as alkaloids and flavonoids found in plant extracts can improve the characteristics of NPs and act as reducing and stabilizing agents [15].

According to recent reports by the World Health Organization, an alarming rise in antibiotic-resistant microorganisms poses a critical threat to global health. Existing antibiotic treatments have become increasingly ineffective owing to several factors, such as poor solubility, instability, and side effects. Consequently, there is an urgent need for novel antimicrobial agents and efficient drug-delivery systems to combat these harmful germs and multidrug-resistant (MDR) species [16]. Nanotechnology offers a promising platform in this regard, owing to the distinctive physicochemical properties, enhanced biodistribution, improved cellular uptake, and targeted delivery potential of NPs [12, 17]. Among these, Co_3O_4NPs are utilized for antibacterial purposes because of their diverse and intriguing physicochemical properties. Biologically synthesized Co_3O_4NPs have potent antibacterial action because of their ability to generate a large amount of highly reduced reactive oxygen species (ROS) and their small crystalline size. Their bactericidal action involves multiple mechanisms, including the disruption of cell membrane integrity, formation of pits and pores, interference with DNA replication, and reduction in the activity of respiratory chain enzymes [18, 19].

NPs can enter the bloodstream regardless of their source, origin, or exposure to the body. Multiple studies have documented that NPs, owing to their diminutive dimensions, can infiltrate the alveolar epithelium, trigger inflammatory responses, and ultimately gain access to the circulatory system. Characterization of the hemocompatibility of NPs involves assessing their hemolytic activity as a marker [20, 21]. Co_3O_4NPs have demonstrated significant efficacy as potential anticoagulant and thrombolytic agents, effectively preventing blood clot formation and dissolving existing clots, making them suitable for thrombosis treatment. The anticoagulant effect of NPs is attributed to their ability to inhibit specific enzymes responsible for thrombin formation within the body [22].

Despite the known pharmacological potential of *Equisetum diffusum*, its application in the green synthesis of Co_3O_4NPs has not been previously explored. Moreover, the systematic evaluation of plant-mediated Co_3O_4NPs for antibacterial, antioxidant, anticoagulant, and thrombolytic activities remains limited. To address this gap, the present study proposes an eco-friendly synthesis of Co_3O_4NPs using an aqueous extract of *E. diffusum*. *E. diffusum* is a popular antibacterial and anti-inflammatory bathing agent for skin disorders [23]. It has been hypothesized that the phytochemicals in the extract can effectively mediate NP formation and enhance their biological performance. The biosynthesized Co_3O_4NPs were characterized using advanced analytical techniques and evaluated for their multifunctional biomedical activities. This work supports sustainable nanomaterial development and aligns with UNSDG Goals 3 and 12 [24, 25]. The green synthesis of Co_3O_4NPs using the *E. diffusum* extract offers a sustainable, cost-effective, and nontoxic alternative to traditional methods, promoting environmental sustainability and advancing health through the development of safe biomedical nanomaterials.

2 | Materials and Methods

2.1 | Reagents and Chemicals Used During Synthesis

E. diffusum D plants were collected from Tehsil Mir Ali, District North Waziristan, Khyber Pakhtunkhwa, Pakistan, and were authenticated by Ms. Naima Huma Naveed, Assistant Professor of Botany at the University of Sargodha, Pakistan. A voucher specimen (SARGU/CHEM-027) was assigned to the plant specimen and deposited in the Herbarium (University of Sargodha-SARGU), Department of Botany, University of Sargodha, Punjab, Pakistan. The plant sample (*E. diffusum D*) was collected from a privately owned land belonging to one of the authors located in North Waziristan, Khyber Pakhtunkhwa, Pakistan, where the species grows naturally. The species is wild, not protected, and not listed as endangered. Therefore, no specific permissions or licenses were required for collection. All procedures complied with relevant institutional, national, and international ethical and legal guidelines.

Laboratory-grade chemicals, cobalt nitrate hexahydrate ($Co(NO_3)_2.6H_2O$) (Sigma-Aldrich), 2, 2-diphenyl-1-picrylhydrazyl hydrate (DPPH) (Sigma-Aldrich), Muller Hilton Agar (Oxide), and ascorbic acid (Sigma-Aldrich) were purchased from a local market. The bacterial strains were obtained from the Biochemistry Lab, University of Sargodha, Pakistan. Deionized water (DI) was used for the solution preparation.

2.2 | Preparation of Aqueous Extract *of Equisetum diffusum*

E. diffusum D plants were collected, washed thoroughly with tap water to remove dust, then with DI, incised into small pieces, and dried in a shady place for 15 days. The dried material was milled into fine powder using a grinder. The aqueous plant extract was prepared following the protocol described by Haq et al. (2021), with some modifications [20]. Briefly, 5 g of plant powder was dissolved in 500 mL of deionized water to prepare a stock aqueous extract and stirred for 5 h at room temperature. The resulting pale-yellow extract was obtained, cooled to room temperature, and filtered three times through a Whatman No. 42 filter paper. The filtrate was then air-dried in an oven set at 45°C and then placed in an amber glass bottle for further use.

2.3 | Fabrication of Cobalt Oxide NPs by *E. diffusum*

The aqueous extract of *E. diffusum* D served as a natural reducing, capping, and stabilizing agent in the synthesis of Co_3O_4NPs. 1 M solution of $Co(NO_3)_2.6H_2O$ (50 mL) was added to 100 mL of an aqueous extract of *E. diffusum* D in an Erlenmeyer flask [21]. Upon continuous stirring on a hot plate at approximately 80°C for 2 h, a shift occurred from yellow to a reddish-brown hue in the solution's color. The solution containing Co_3O_4NPs was subjected to three washes with DI water before being heated in an oven at 70°C for 12 h in order to obtain dried precipitates. The dried material was subsequently calcined at 400°C for 2 h in a muffle furnace to enhance crystallinity. The resulting dark brown Co_3O_4NPs obtained were stored in an airtight jar for further characterization and mentioned as ED@Co_3O_4NPs.

2.4 | Characterization

A combination of spectroscopic and microscopic techniques was employed to characterize the biosynthesized ED@Co_3O_4NPs. UV–Visible spectrophotometry (UV-1700 Pharmspec, Shimadzu) was used to evaluate the optical characteristics of the biosynthesized ED@Co_3O_4NPs in the range of 250–700 nm. FTIR analysis was performed to detect the functional groups present in the samples. The surface morphology, size, and shape of Co_3O_4NPs were analyzed by SEM, and dynamic light scattering (DLS), while zeta potential measurements were carried out using a Zetasizer (Malvern Zetasizer Nano ZS). The crystal size and purity of the ED@Co_3O_4NPs were confirmed using XRD (JDX-3532, JEOL, Tokyo, Japan). Energy-dispersive x-ray spectroscopy (EDX) was used to determine the elemental composition of the samples. Finally, a thermogravimetric analysis [simultaneous thermal analyzer (TGA/DSC) SDT 650] was used to assess the thermal stability of ED@Co_3O_4NPs at room temperature and 900°C. TGA breakdown profiles were measured under nitrogen gas at a rate of 10°C min^{-1}. Using a heating rate of 10°C min^{-1} under a nitrogen environment, the DSC experiments were executed using a device (SDT 650) in a temperature range of ambient to 500°C [26].

2.5 | Antibacterial Potential

The antibacterial potential of ED@Co_3O_4NPs was evaluated using a well diffusion method following the protocol of Roheen et al. (2025), with a few modifications [27]. The Petri dishes were autoclaved at 120°C for 20 min at 15 psi after dissolving 5 g of Muller-Hinton agar (MHA) in 100 mL of DI. The autoclaved agar solution was then poured into sterilized Petri plates and allowed to solidify for 15 min. Before the antibacterial activity, subcultures were prepared from pure cultures of *Pseudomonas aeruginosa* (ATCC 10145), *Escherichia coli* (ATCC 10536), and *Staphylococcus epidermidis* (ATCC 12228) and incubated at 37°C for 24 h. Then, using the streak plate method, bacterial cultures were equally spread on sterilized agar plates with cotton swabs. Four 6-mm wells were formed in each Petri plate using a cork borer. A 20-μL solution of ceftriaxone (1 mg/mL, positive control), ED@Co_3O_4NPs (1 mg/mL), *E. diffusum* plant extract (1 mg/mL), and DI (negative control) were poured into separate wells, alphabetically labeled as A, B, C, and D, respectively, and placed in an incubator at 37°C for 24 h. The procedure was performed in the microbiology lab under aseptic conditions in a laminar-flow cabinet to prevent contamination.

The minimum inhibitory concentration (MIC) of the ED@Co_3O_4NPs was performed using the microdilution method. Briefly, serial twofold dilutions of the ED@Co_3O_4NPs were prepared in Muller-Hinton broth (MHB) between 10 and 70 μg/mL. The bacterial strains *P. aeruginosa*, *E. coli*, and *S. epidermidis* were cultured to the logarithmic phase, and an inoculum of approximately 1×10^6 CFU/mL was added to each test tube. The test tubes were kept in an incubator at 37°C for 24 h. The MIC was defined as the lowest concentration of ED@Co_3O_4NPs preventing visible growth of bacteria.

Following the determination of the MIC, an aliquot from each well without visible growth was plated on MHA for evaluation of bactericidal activity. The lowest level of ED@Co_3O_4NPs that led to the total elimination of colony formation was established as MBC and occurred at 37°C after a 24-h incubation.

2.6 | Antioxidant Potential Using 2,2-Diphenyl-1-Picrylhydrazyl (DPPH) Assay

The DPPH scavenging potential of the green fabricated ED@Co_3O_4NPs was evaluated using the modified protocol of Assad et al. (2025) [28]. Varying concentrations of ED@Co_3O_4NPs (100, 150, 200, 250, and 3000 μL) (1 mg/mL) were mixed with 3 mL of a 0.2 M ethanolic DPPH (4 mg/100 mL) solution. Absolute ethanol (99.98%) was added to each sample to obtain a final volume of 10 mL. Reference samples were prepared by dissolving different concentrations of ascorbic acid following the same protocol mentioned above. The solutions were incubated at 25°C for 30 min in the dark. The absorbance was measured at 517 nm for both the test and reference samples (ascorbic acid). The percentage scavenging activity (%RSA) of ED@Co_3O_4NPs was determined using the following equation:

$$\%\mathrm{RSA} = \left((\mathrm{Ac\,at\,517nm} - \mathrm{As\,at\,517nm})/(Ac\,517\,\mathrm{nm})\right) \times 100, \quad (1)$$

where As is the sample absorbance and Ac is the control's absorbance.

2.7 | Ferric Reducing Antioxidant Power (FRAP) Assay

Using the FRAP assay, the aqueous extract of *E. diffusum* D, which induces the formation of Co_3O_4NPs, demonstrated significant antioxidant activity. The FRAP assay was performed following the protocol described by Gul et al. (2025), with slight modifications [29]. Co_3O_4NPs were diluted in DI to concentrations ranging from 100 to 300 μL (1 mg/mL). Ascorbic acid served as the standard, with reference solutions of 100, 150, 200, 250, and 300 μL (1 mg/mL).

The phosphate buffer (pH 6.6) was prepared by mixing 0.2 g of potassium chloride, 1.44 g of disodium hydrogen phosphate, 8 g of sodium chloride, and 0.24 g of potassium dihydrogen phosphate in 500 mL of DI. HCL was added to adjust the pH. Phosphate buffer (pH 6.6) (2.5 mL) and 1% $K_3Fe(CN)_6$ (2.5 mL) were mixed with ED@Co_3O_4NPs, samples, and controls for the assay. After 5 min of vortexing, the mixture was incubated at 50°C for 20 min. Following the incubation, 2.5 mL of 10% TCA was added and the mixture was centrifuged for 10 min at 3000 rpm. The supernatant was collected, and DI (2.5 mL) was added. To develop a colored solution, 0.5 mL of 0.1% ferric chloride was added. The absorbance of the samples and reference solutions was determined at 711 nm using a UV–Visible spectrophotometer. The experiment was performed three times, and the mean ± standard deviation was calculated to describe the results. The scavenging activity was estimated using the following equation [30]:

$$x = \frac{y}{0.0024}, \mathrm{R2} = 0.969. \quad (2)$$

2.8 | Hemolytic Potential

In vitro hemolysis assay of ED@Co_3O_4NPs was determined using the protocol described by Das and Saikia (2023) with slight modifications [31]. Fresh human blood samples were collected after obtaining consent from the author and ethical approval from the Biosafety and Ethical Review Committee, University of Sargodha, Pakistan (Ref no: SU/ORIC/2073), added to an

anticoagulant vial containing sodium heparin, and centrifuged at 3000 rpm for 5 min to separate plasma. After removing the supernatant plasma from the blood, the remaining pellets were suspended in 10 mL of chilled (4°C) PBS buffer of pH 7.4 and centrifuged thrice to obtain a plasma-free pellet. Different concentrations of ED@Co_3O_4NPs (0.25–5 μg/mL) were added to test tubes containing 2 mL of RBC suspension in each test tube. The positive control in this experiment was Triton X-100, whereas PBS was used as the negative control. After that, the test tubes were carefully inverted and incubated for 90 min at 25°C. The absorbance of the supernatant was measured at 540 nm, using PBS as a blank. The percentage of hemolysis (%) was calculated using the following equation:

$$\%\text{hemolysis} = \frac{OD_s - OD_c}{\text{OD positive control} - \text{OD negative control}} \times 100. \quad (3)$$

2.9 | Anticoagulant and Thrombolytic Potential

The anticoagulant activity of ED@Co_3O_4NPs was performed using a modified protocol described by Ajarem et al. (2021) [22]. Four test tubes were taken, and 1 mL of freshly collected human blood was added to each test tube, followed by the addition of varying concentrations (20, 30, and 40 μg/mL) of ED@Co_3O_4NP solution in three test tubes. The fourth test tube served as the control. The test tubes were then incubated at 37°C for 1 h to check for clot formation. The thrombolytic activity of ED@Co_3O_4NPs was determined using the procedure described by Azeez et al., (2020) [32]. A small drop of fresh blood was placed on a glass slide and allowed to remain for 20 min to form a clot. Then, 20–40 μg/mL of ED@Co_3O_4NPs was gently added onto each clot. The extent of clot dissolution was observed and recorded, indicating the thrombolytic efficiency of the ED@Co_3O_4NPs.

2.10 | Statistical Analysis

Graphical and numerical data were analyzed using Excel 2016 and Origin Pro 2021. All experiments were performed in triplicate ($n = 3$), and results are expressed as mean ± standard deviation (SD). For antibacterial activity, one-way analysis of variance (ANOVA) was performed to compare the differences in mean zones of inhibition among the different treatments (positive control, ED@Co_3O_4NPs, and *E. diffusum* extract) for each bacterial strain. Following a significant ANOVA result ($p < 0.05$), Tukey's honestly significant difference (HSD) post hoc test was used for all-pairwise comparisons to identify specific differences between treatment groups. Bartlett's test was used to assess the homogeneity of variances. Statistical computations were performed using Statistix 8.1 software.

3 | Results and Discussion

3.1 | Green Synthesis of ED@Co_3O_4NPs

The green synthesis approach applied in the current study to prepare Co_3O_4NPs with *E. diffusum* D extract was found to be efficient, inexpensive, and environmentally friendly. The reduction, capping, and stabilizing role of *E. diffusum* D extract are critical for the successful synthesis of Co_3O_4NPs [33]. The aqueous extract of *E. diffusum* D is rich in several bioactive compounds (alkaloids and flavonoids) that are responsible for cobalt nitrate hexahydrate reduction and stabilization of NPs [34]. In a conical flask, 100 mL of *E. diffusum* D extract was mixed with 50 mL of a 0.2 M solution of $Co(NO_3)_2{\cdot}6H_2O$ during synthesis. The solution was constantly stirred using a hot plate at approximately 80°C for 2 h. A marked color change (yellow-red-brown) was observed, confirming the formation of Co_3O_4NPs. The solution was then washed with DI water three times to remove any unreacted materials and impurities. The washed solution was air-dried at 70°C for 12 h to obtain dried precipitates. Then, it was crushed and calcined at 400°C for 2 h to improve crystallinity (the dark-brown Co_3O_4NP product in Figure 1).

3.2 | UV–Vis Spectroscopy

The synthesis of the ED@Co_3O_4NPs was analyzed using a UV–Visible spectrophotometer (Figure 2). The UV–Vis spectrum of the prepared ED@Co_3O_4NPs displayed an absorption peak at 323 nm, which is characteristic of ED@Co_3O_4NPs. This peak is due to the surface plasmon resonance (SPR) band of the particles, while the broad maximum indicates the large size distribution of these particles [35]. This absorption is probably ascribed to the charge transfer between O and Co ions in the spinel lattice and is consistent with the UV–Vis spectra of Co_3O_4 nanostructures produced by other green methods reported [31, 36]. The ED@Co_3O_4NPs were synthesized by reducing cobalt (II) nitrate hexahydrate with an aqueous extract of *E. diffusum* D, which acted as a capping, reducing, and stabilizing agent [37]. The green synthesis of Co_3O_4NPs entails the reduction of cobalt ions to neutral cobalt atoms, followed by nucleation and growth processes. The resulting particles were stabilized using bioactive phenolic molecules found in plant extracts [38]. Phenolic compounds possess carboxylic and hydroxyl groups, which have a strong tendency to form bonds with metals. Upon formation of a chelate, the hydrogen atom is eliminated from the ortho position of the phenolic hydroxyl group, leading to the formation of a structure resembling a semiquinone. As a result, Co(II) is converted into Co atoms at the nanoscale because of the bioactive chemicals acting as capping agents [39, 40].

3.3 | XRD Analysis of ED@Co_3O_4NPs

The crystalline structure of the biosynthesized ED@Co_3O_4NPs was confirmed by x-ray diffraction (XRD) analysis, as shown in Figure 3(a). The diffraction peaks observed at $2\theta = 31.90°$ (220), 35.38° (311), 38.03° (222), 46.26° (400), 56.44° (511), and 76.36° (622) correspond well with the standard JCPDS card No. 42-1467, confirming the formation of spinel-phase ED@Co_3O_4NPs [41]. However, the peaks at $2\theta = 19.86°$, 21.72°, 29.36°, and 47.94° did not directly match the Co_3O_4NP reference, suggesting the possible presence of plant extract within the sample [42]. The average crystallite size (D) of the biosynthesized ED@Co_3O_4NPs was calculated using the Scherrer equation [43] as follows:

$$D = \frac{k\lambda}{\beta \text{Cos}\theta}, \quad (4)$$

where K is the Scherrer constant with a value of 0.9. The symbol λ indicates the wavelength of the x-ray source, which was 0.15406 nm. The radian degree value of the FWHM of the

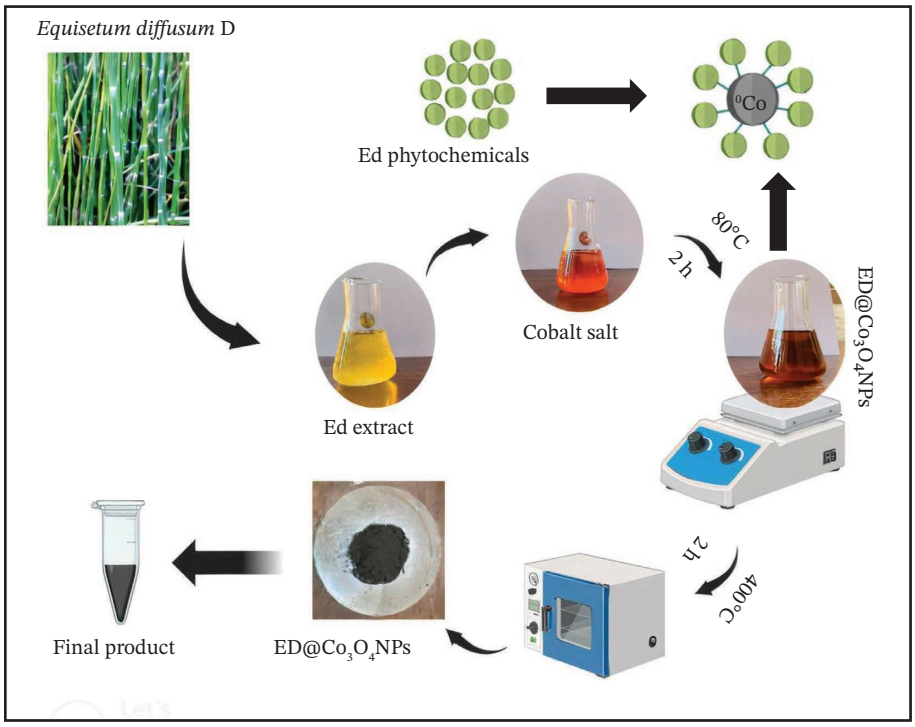


FIGURE 1 | Schematic representation of biosynthesized ED@Co3O4 NPs.

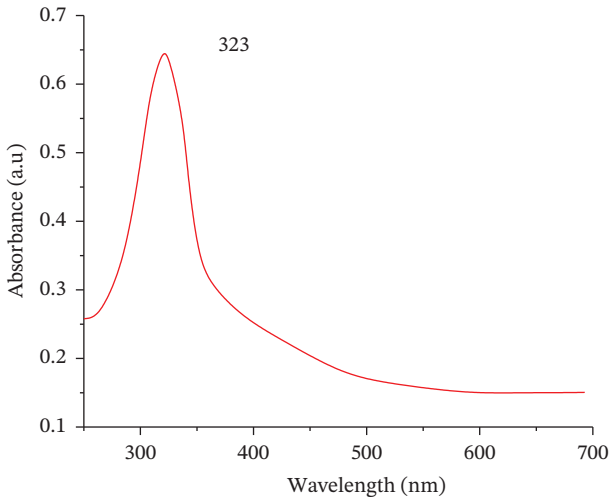


FIGURE 2 | UV–vis spectroscopy of the biosynthesized ED@Co_3O_4NPs.

analyzed peaks is represented by the symbol β. In addition, θ represents the orientation of the peak in radians. The biosynthesized ED@Co_3O_4NPs have a nanocrystalline structure, with an average size of approximately 15.17 nm, confirming their nanoscale nature. The absence of extra diffraction peaks indicates high-phase purity, which is consistent with previously published Co_3O_4 NP studies [31, 44].

The dislocation density (δ) obtained from the XRD measurements was determined using the following equation:

$$\delta = \frac{1}{D2}, \tag{5}$$

where D is the crystallite size, calculated using the Scherrer equation. Given that the crystallite size D is approximately 15.17 nm, the dislocation density of the synthesized ED@Co_3O_4NPs is approximately $4.35 \times 10^{15}\ m^{-2}$.

The interplanar spacing (d) for a specific set of crystal planes was calculated using Bragg's equation:

$$n\lambda = 2d\sin\theta, \tag{6}$$

where λ denotes the wavelength. The calculated value of the interplanar spacing is 2.48 Å for the high-intensity peak ((511)), and the average lattice parameter (a) was calculated using the following equation:

$$d = \frac{a}{\sqrt{h^2 + k^2 + k^2}} \tag{7}$$

The peaks of the XRD pattern of the ED@Co_3O_4NPs are consistent with those of the standard reference patterns for Co_3O_4, indicating that the NPs were successfully synthesized and the average lattice parameter obtained from the peaks was approximately 0.8167 nm, indicating a uniform crystal structure in the synthesized solid.

3.4 | FTIR Analysis of Biosynthesized ED@Co_3O_4NPs

To compare the different functional groups and stretching vibrations between the FTIR spectra of the plant extract and the synthesized ED@Co_3O_4NPs, the key peaks and their corresponding functional groups were recorded using FTIR analysis, as shown in Figure 3(b).

In the FTIR spectrum of the plant extract, a broad absorption peak at approximately 3454 cm^{-1} was attributed to the O–H stretching vibrations of hydroxyl groups in phenolic and alcoholic compounds. The peaks at approximately 2900 cm^{-1} are C–H stretching vibrations, which are characteristic of organic

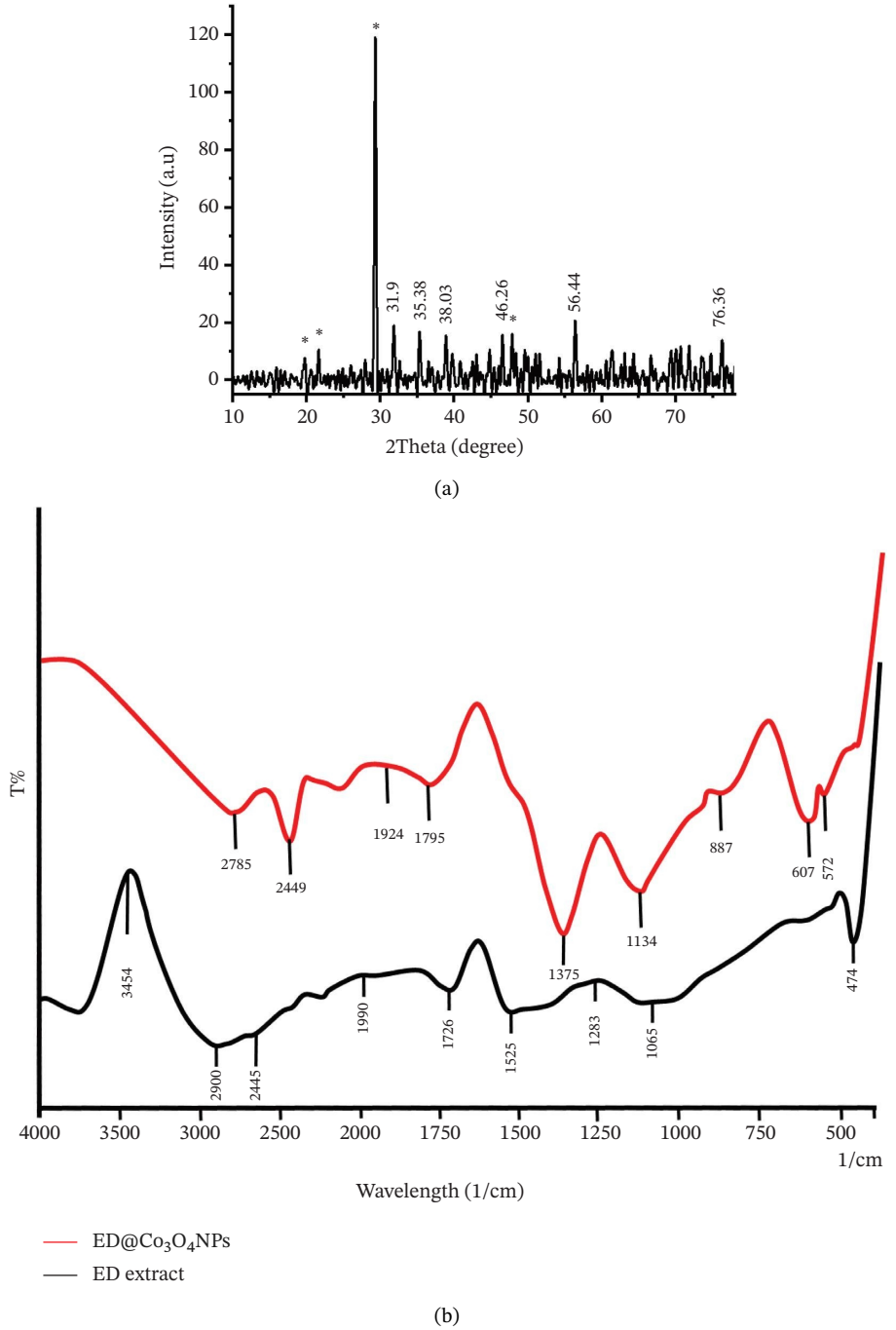


FIGURE 3 | (a) XRD pattern of ED@Co_3O_4NPs and (b) FTIR spectrum of the synthesized ED@Co_3O_4 NPs.

compounds [45]. The intense peak at ca 1726 cm^{-1} indicates the presence of carbonyl moieties (C=O) such as aldehyde, ketone, or carboxylic acids [46]. The region below 1000 cm^{-1} contains various peaks that are indicative of complex organic molecules.

In contrast, the FTIR spectrum of the synthesized ED@Co_3O_4NPs shows additional peaks that confirmed the formation of metal oxide bonds. The peaks observed around 572 and 607 cm^{-1} indicate Co–O stretching vibrations, confirming the presence of cobalt oxide in the NPs [47–49]. Similar binding-group patterns have been reported in other plant-mediated Co_3O_4NP syntheses [50]. The presence of these peaks, along with those from the plant extract, as shown in Table 1, suggests that the biomolecules from the plant extract acted as capping agents, stabilizing the NPs and facilitating their synthesis [46].

3.5 | Scanning Electron Microscopy (SEM) Analysis

The SEM of the green synthesized ED@Co_3O_4NPs demonstrates the presence of uniformly distributed, nearly spherical particles with minimal signs of agglomeration, indicating excellent stability and homogeneous morphology as shown in Figures 4(A), 4(B), 4(C), 4(D), 4(E). The spherical structure of the Co_3O_4NPs is attributed to the controlled processes of nucleation, growth, and aggregation during synthesis [47]. Plant derivatives control the

TABLE 1 | FTIR spectrum data of ED extract and ED extract–mediated ED@Co_3O_4NPs.

S.NO	Functional group (ED extract)	Functional group (ED@Co_3O_4NPs)	Functional group
1	3454	___	O–H stretch (alcohol, phenol)
2	2900	2785	C–H stretch (alkanes)
3	2445	2449	N–H stretch (amines)
4	1990	1924	C=O stretch (aldehydes, ketones)
5	1726	1795	C=O stretch (carbonyls)
6	1525	___	N–O asymmetric stretch
7	1383	1375	C–H bend (alkanes)
8	1065	1134	C–N stretch (amines)
9	___	887	C–H bend (aromatics)
10	___	607, 572	M–O stretch (metal oxides)
11	474	___	halogen stretching

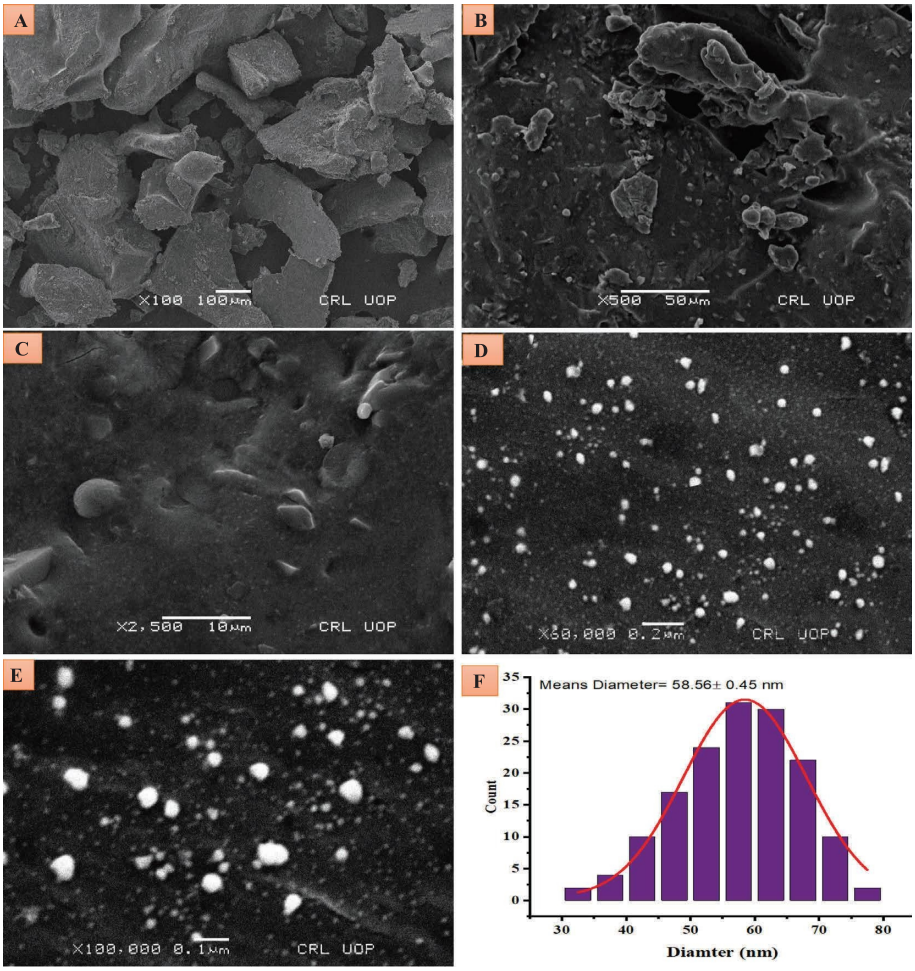


FIGURE 4 | (A–E) SEM analysis of ED@Co_3O_4NPs at different magnifications. (F) Size distribution histogram of the biosynthesized ED@Co_3O_4NPs.

nucleation, growth, and structuring of NPs [51]. The particle size distribution histogram indicated the average particle diameter of 58.56 nm, together with a narrow standard deviation of 0.45 nm, which confirms the presence of a uniform particle size as shown in Figure 4(F).

Spherical geometry provides convenient homogeneous biological interactions (e.g., cell uptake and biointeraction). The moniform morphological distribution of plant-mediated oxide NPS has been reported in previous studies and is an indication for well-controlled synthesis [31, 52]. The use of plant extracts as reducing and capping

agents in green synthesis methods renders them eco-friendly, cost-effective, and biocompatible because they avoid toxic chemicals/solvents. This environment-friendly approach makes NPs more beneficial for medicinal and other purposes, in which natural phytochemicals are used for highly qualitative NPs.

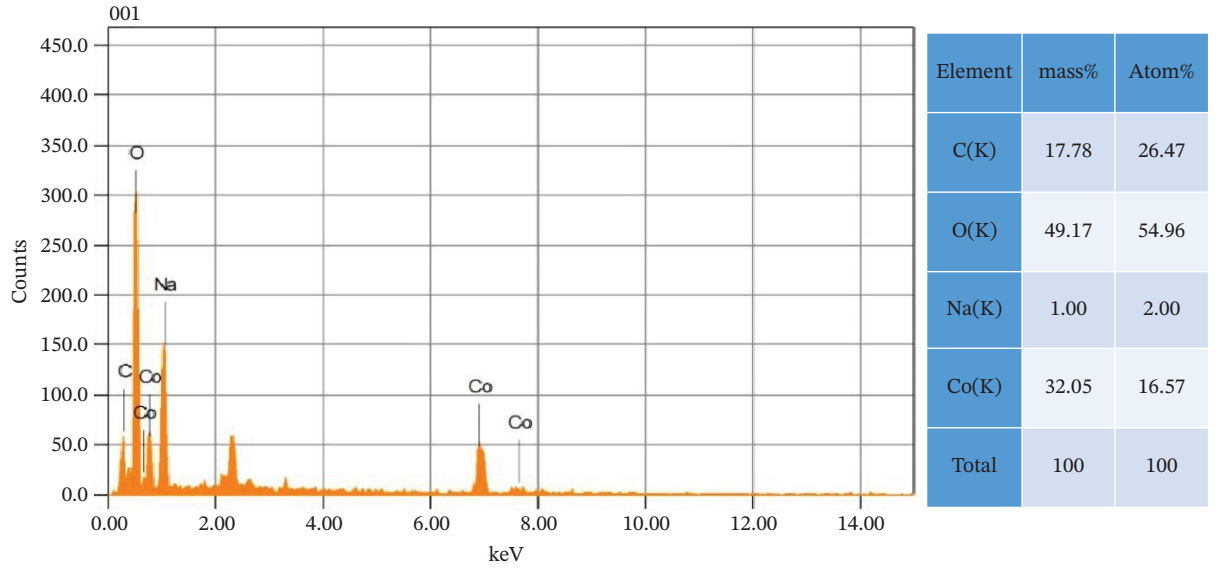
3.6 | EDX Analysis of the Green Synthesized ED@Co_3O_4NPs

The EDX analysis of the green synthesized ED@Co_3O_4NPs confirmed the elemental composition of 17.78% carbon (C), 49.17% oxygen (O), 1.00% sodium (Na), and 32.05% cobalt (Co) by mass, as depicted in Figure 5(a). The strong oxygen and cobalt signals validate the successful formation of Co_3O_4NPs, while the carbon and sodium peaks were attributed to phytoconstituents from the *E. diffusum* extract, which acted as reducing, capping, and stabilizing agents during NP synthesis. This observation is consistent with recent studies that employed plant extracts, such as rosemary, for the eco-friendly and cost-effective synthesis of Co_3O_4NPs [53]. These studies confirmed the elemental composition and demonstrated that such NPs possess unique properties, making them suitable for various applications, including catalysis and biomedicine, owing to their stability and non-toxicity at specific concentrations [54].

3.7 | DLS Analysis

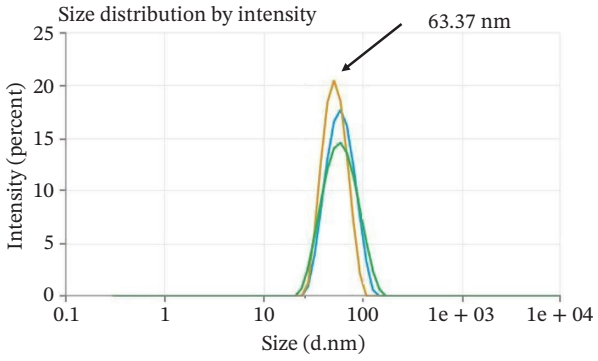
The DLS results of the green fabricated ED@Co_3O_4NPs NPs show an average particle size of 63.37 nm, which is slightly higher than that observed in the SEM analysis (58.56 nm), as presented in Figure 5(b). This discrepancy can be explained by the aforementioned difference between DLS measurements, which mostly provide hydrodynamic diameters that are better than the SEM sizes [55, 56]. These results indicate that the green synthesis technique can be efficiently employed for the production of Co_3O_4NPs with particle sizes suitable for applications in catalysis, biomedicine, and environmental protection because of their high surface area and reactivity.

The zeta potential measurement of the green synthesized ED@Co_3O_4NPs reveals −32 mV, indicating the suspension stability of the NPs as shown in Figure 5(c). This negative zeta potential is attributed to the high electrostatic repulsion among the particles, which plays a role in maintaining a stable colloidal system. It has been reported that green-prepared Co_3O_4NPs generally have a negative zeta potential. Al-Qasmi (2022) found that the green-synthesized Co_3O_4NPs with *R. officinalis* Linn extract have excellent stability properties, as evidenced by zeta potentials (negative), which guarantee colloidal conditions and dispersive effectiveness [53]. Another experiment conducted by Mehrafza

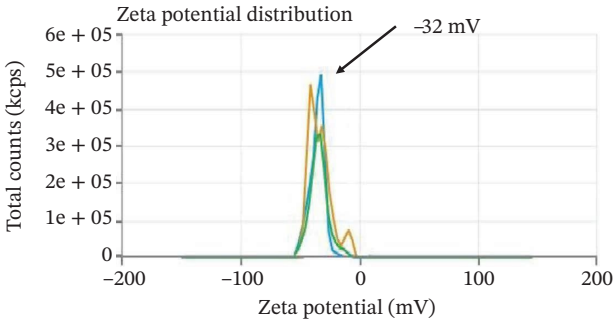


Element	mass%	Atom%
C(K)	17.78	26.47
O(K)	49.17	54.96
Na(K)	1.00	2.00
Co(K)	32.05	16.57
Total	100	100

(a)



(b)



(c)

FIGURE 5 | (a) EDX spectra of ED@Co_3O_4NPs, (b) DLS zeta sizer, and (c) zeta potential of the green synthesized ED@Co_3O_4NPs.

et al. (2024) in the green synthesis of Co_3O_4NPs using *Bacillus megaterium* showed a negative zeta potential, which is indicative of the stability of the NPs in suspension, an important characteristic for their application in different areas such as catalysis and biomedicine [57].

3.8 | TGA and DSC Analysis of Green Synthesized ED@Co_3O_4NPs

The thermal stability, decomposition behavior, and phase transitions of green synthesized ED@Co_3O_4NPs were elucidated by TGA. Preliminary TGA measurements indicated a slight weight loss of 1.27 mg (7.092%) in the range from 15.60 to 200°C due to evaporation of water and volatile organics formed during synthesis, respectively. A considerable amount of weight loss (15.031 mg, 16.69%) observed around at 343.09°C corresponds to the decomposition of organic elements derived from botanical extract, resulting in cobalt oxide generation. Additional mass loss was observed below 815.9°C to reach a final value of 13.014 mg (27.58%), denoting the elimination of organic matter remnants and complete crystallization into Co_3O_4 with a final residue left at 900°C of 12.841 mg (28.48%). DSC analyses exhibit physical strict state transitions as derived from glass transition temperature located at 259.97°C, whereas the onset of oxidation is signaled at 220.78°C, which is important with respect to precursor superoxidation._softc1:specified grade XC400 biterocks; digital/D41 The exothermic process at 447.34°C with an enthalpy change of 2670.5 J/g is ascribed to the crystallization and stabilization of ED@Co_3O_4NPs (Figure 6). These investigations confirmed the thermophysical properties and stability of the NPs, which could find practical applications in catalysis, biomedicine, and the environment.

3.9 | Antibacterial Activity

Infections caused by pathogenic organisms are a serious global health threat, particularly in developing nations, where the misuse of antibiotics is prevalent [58]. This has also contributed to the development of MDR strains that are resistant to several drugs. The development of drugs to combat pathogenic bacterial strains, including MR strains, is of great significance in the fight against infectious illnesses. In recent years, scientists have focused on NPs and microscopic particles that exhibit toxicity against harmful microbial strains [59, 60]. In particular, NPs synthesized via biogenic pathways have been the subject of many recently published investigations for their antibacterial potential, with promising findings against a wide range of bacterial strains [61, 62].

The antibacterial activity of ED@Co_3O_4NPs was evaluated against three bacterial strains, *Pseudomonas aeruginosa* (ATCC 10145), *Escherichia coli* (ATCC 10536), and *Staphylococcus epidermidis* (ATCC 12228). The biosynthesized ED@Co_3O_4NPs showed a significant zone of inhibition of 25, 22, and 12 mm against *P. aeruginosa*, *E. coli,* and *S. epidermidis*, respectively, suggesting potential antibacterial properties. With reference to *S. epidermidis*, the ED@Co_3O_4NPs also resulted in an inhibition zone that is smaller than the other two but marked by a substantial antibacterial action (see Figure 7).

The positive control (ceftriaxone 1 mg/mL) exhibited significant inhibition zones of 27.0 ± 1.0 mm against *P. aeruginosa*, 21.0 ± 1.0 mm against *E. coli*, and 13.0 ± 1.0 mm against *S. epidermidis*. Similarly, the *E. diffusum* plant extract presented moderate activity when tested alone against these strains, with inhibition zones of 17.0 ± 1.0 mm against *P. aeruginosa*, 17.0 ± 1.0 mm against *E. coli*, and 9.0 ± 1.0 mm against *S. epidermidis*. These data demonstrate the wide-spectrum antimicrobial activity

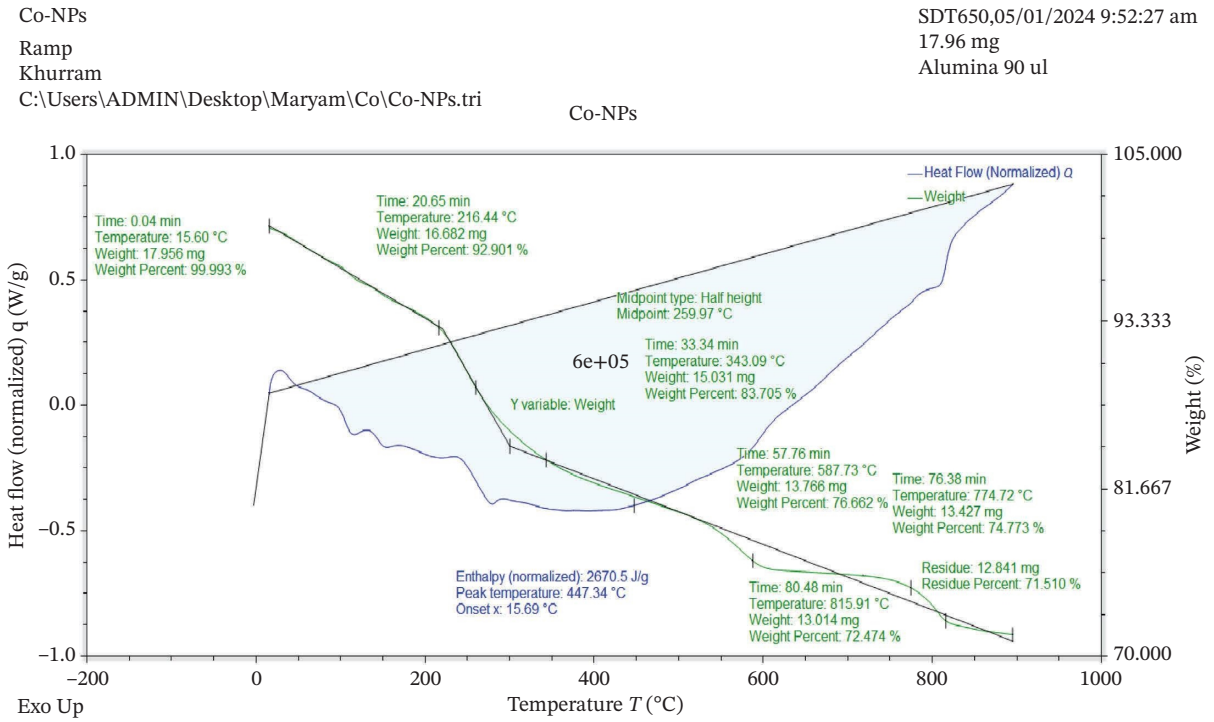


FIGURE 6 | TGA/DSC analysis of the green synthesized ED@Co_3O_4NPs.

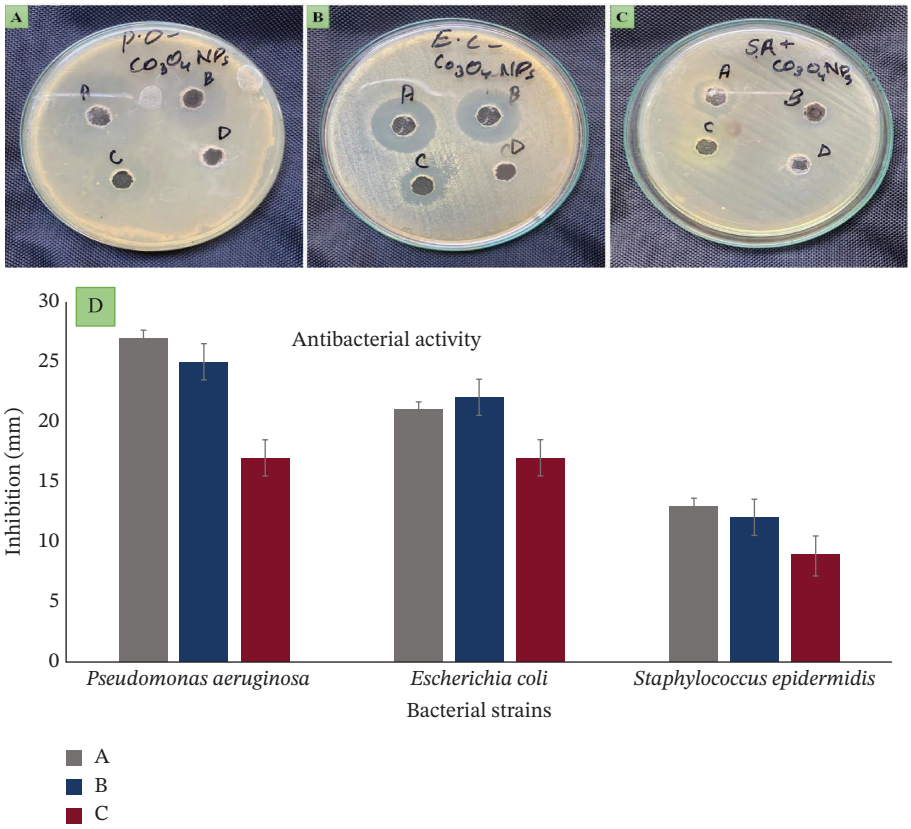


FIGURE 7 | Antibacterial activity: (A) *P. aeruginosa* (ATCC 10145), (B) *E. coli* (ATCC 10536), (C) *S. epidermidis* (ATCC 12228), and (D) a graphical representation of the mean inhibition zones (mm ± SD) for (A) positive control (ceftriaxone 1 mg/mL), (B) ED@Co_3O_4NPs (1 mg/mL), and (C) *Equisetum diffusum* extract (1 mg/mL) against the three bacterial strains. Statistical significance for pairwise comparisons between treatments within each bacterial strain was determined by one-way ANOVA followed by Tukey's HSD post hoc test ($p < 0.05$).

of ED@Co3O4NPs and confirm that our NPs may be potential candidates as powerful antibacterial agents.

These data demonstrate the wide-spectrum antimicrobial activity of ED@Co_3O_4NPs, confirming their efficacy against both Gram-negative (*P. aeruginosa*, *E. coli*) and Gram-positive (*S. epidermidis*) bacteria. The comparable performance of ED@Co_3O_4NPs to the standard antibiotic ceftriaxone (statistically confirmed by Tukey HSD for all tested strains) highlights their potential as powerful antibacterial agents.

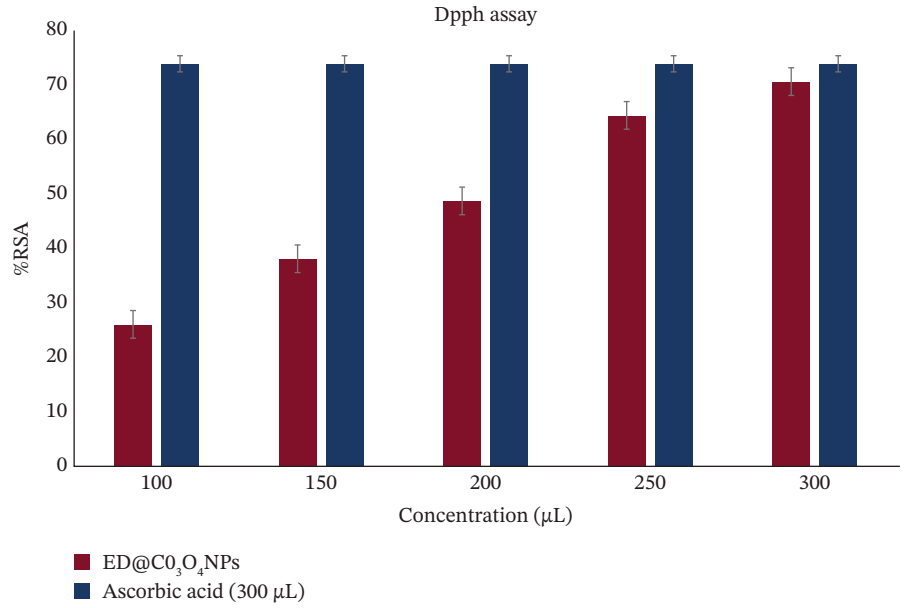
Several mechanisms have been proposed to explain the antibacterial activity of NPs [63]. In these processes, NPs attach to the cell wall of microbes, which disrupts the cell wall, allows NPs to infiltrate the cell membrane, and eventually causes membrane disintegration [64, 65] and damage to proteins, enzymes, and DNA [66, 67]. NPs generate ROS, which cause oxidative stress in the cell and affect various metabolic pathways of the cell, leading to cell lysis [68, 69]. Similar to recent reports of tetrazole-based metal-coordinating systems demonstrating strong metal–biomolecule interactions and biological activity, the observed antibacterial performance of ED@Co_3O_4NPs may also be influenced by surface-mediated metal ion interactions and oxidative stress mechanisms [70, 71]. Antibacterial activity was evaluated to determine the biomedical relevance of the biosynthesized Co_3O_4NPs, as cobalt oxide nanostructures are known to exert antimicrobial effects through ROS generation and membrane disruption mechanisms. Furthermore, the medicinal background of *Equisetum diffusum* suggests that plant-mediated synthesis may influence the surface chemistry and enhance biological performance, making antibacterial assessment essential for validating the functional potential of the synthesized nanomaterial.

The MIC of the ED@Co_3O_4NPs was measured by microdilution method. MIC results were 20 for *P. aeruginosa*, 20 for *E. coli*, and 30 μg/mL for *S. epidermidis* as shown in Table 2. Among the strains tested, *P. aeruginosa* showed the lowest MIC, indicating that it was more susceptible to ED@Co_3O_4NPs than other strains. Aliquots from the test tube, which showed no visible growth, were plated onto MHA to determine the minimum bactericidal concentration (MBC). MBC values obtained for *P. aeruginosa*, *E. coli,* and *S. epidermidis* were 20 μg/mL, 40 μg/mL, and 50 μg/mL, respectively, as shown in Table 2. The results indicated the

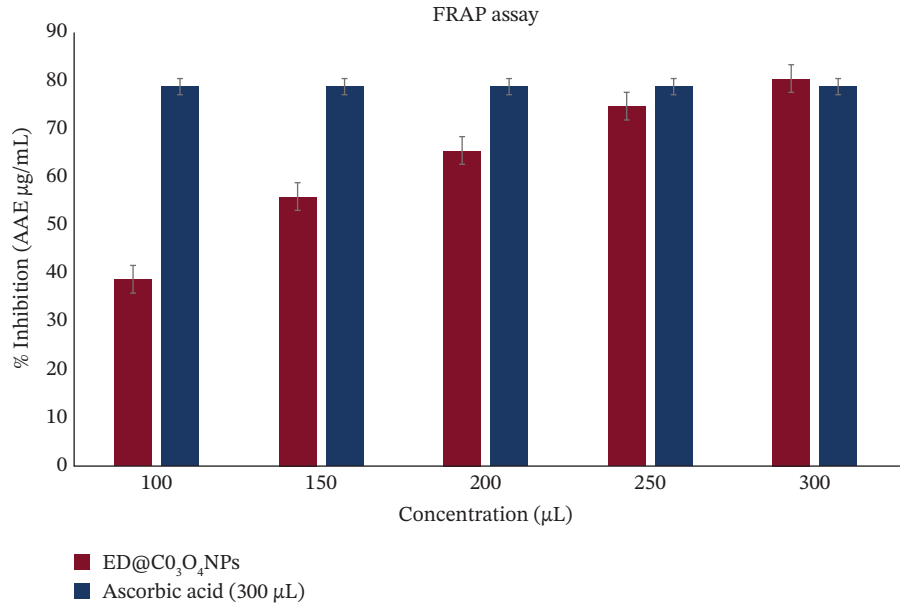
TABLE 2 | Antibacterial activity of ED@Co_3O_4NPs against different bacterial strains.

Bacterial strain	ZOI (mm)	MIC (μg/mL)	MBC (μg/mL)
P. aeruginosa	25	20 ± 1.5	20 ± 1.2
E. coli	22	20 ± 1.3	40 ± 1.8
S. epidermidis	12	30 ± 2.0	50 ± 2.5

Note: Values of ZOI, MIC, and MBC for *P. aeruginosa*, *E. coli,* and *S. epidermidis*, along with their respective standard deviations (SDs).



(a)



(b)

FIGURE 8 | Antioxidant activity of the green synthesized ED@Co_3O_4NPs: (a) DPPH assay and (b) FRAP assay.

requirement of the lowest concentration of ED@Co_3O_4NPs to obtain bactericidal activity against *P. aeruginosa*, whereas Gram-positive *S. epidermidis* was inhibited with the highest MBC value implying it to be least susceptible.

3.10 | Antioxidant Activity

DPPH assay is a widely used method for evaluating the free radical scavenging potential of a compound. DPPH was chosen as the model assay for free radical scavenging activity because it is a highly stable lipophilic radical [72]. The percentage inhibition activity of NPs was between 24.735% and 85.457%, as depicted in Figure 8(a). The findings were compared to those for the ED@Co3O4NPs and ascorbic acid (300 μL; standard) layers. The scavenging (%) of DPPH significantly depends on the concentration (in μL) of ED@Co_3O_4NPs, and an upward trend in percentage was observed with increasing volume, i.e., 38.75–80.41% (100–300 μL), which reflects that as the ED@

TABLE 3 | % Hemolytic activity of the biosynthesized ED@Co_3O_4NPs.

Sample concentration (μg/mL)	OD at 540 nm	% Hemolysis
0.5	0.117	0.10
1	0.119	0.19
2	0.124	0.39
2.5	0.163	2.03
5	0.204	3.76

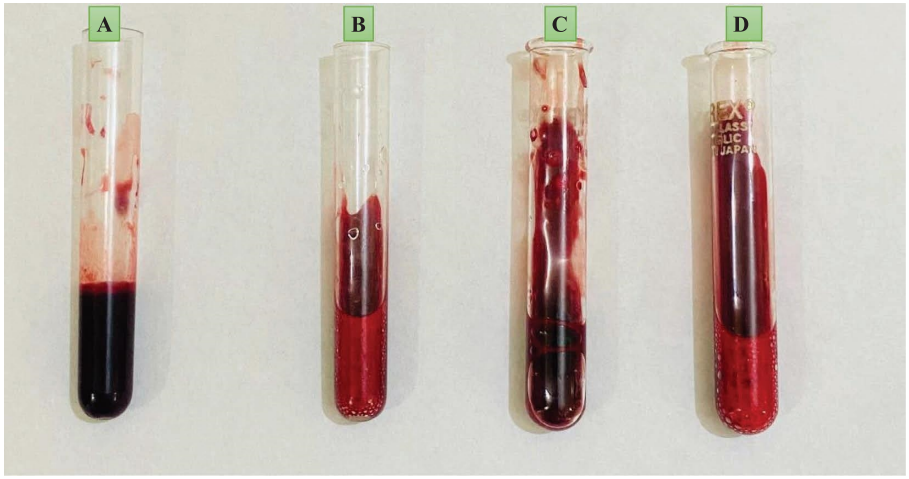
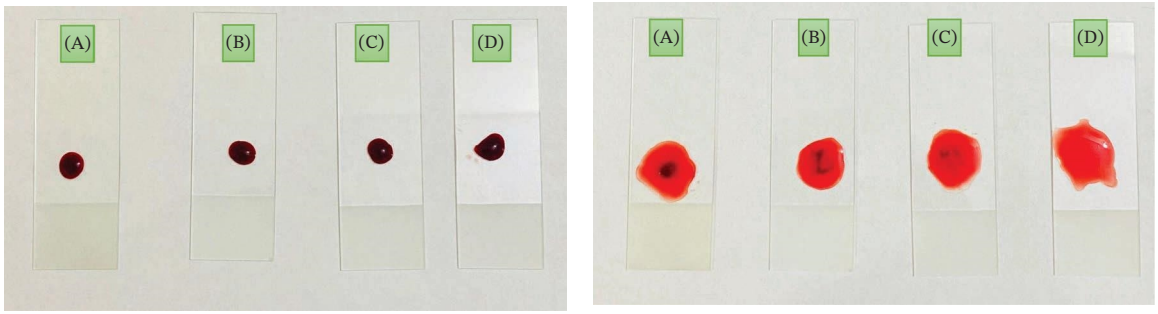


FIGURE 9 | Anticoagulant activity of the green ED@Co_3O_4NPs.



(a) (b)

FIGURE 10 | Thrombolytic analysis of biosynthesized ED@Co_3O_4NPs.

Co_3O_4NP concentration increases, its potential for neutralization of free radicals also increases. Furthermore, the antioxidant activity of ED@Co_3O_4NPs is higher than that of ascorbic acid while exhibiting stable and relatively high scavenging (78.75% at 300 μL), indicating potential for use as antioxidants.

The FRAP assay is based on the ability of samples to reduce ferric ions to ferrous ions. As the FRAP test is concerned, ED@Co_3O_4NPs at different concentrations exert increasing reducing power values from 26.05 mg AAE/g (100 μL) to 70.44 mg AAE/g (300 μL). Ascorbic acid, used as a standard at a single concentration of 300 μL, demonstrated a consistently high reducing power of 73.9 mg AAE/g. At 300 μL, the reducing power of ED@Co_3O_4NPs is nearly comparable to that of ascorbic acid as shown in Figure 8(b). This indicates that ED@Co_3O_4NPs possess strong antioxidant properties, especially at higher concentrations, and could be considered as effective as ascorbic acid in reducing ferric ions in an FRAP assay [73].

3.11 | In Vitro Hemolytic Potential

The hemolytic activity of the ED@Co_3O_4NPs was systematically evaluated by measuring the optical density (OD) at 540 nm across a range of concentrations. Phosphate-buffered saline (PBS) served as the negative control with an OD of 0.11, and Triton X-100 (TX100) was used as the positive control, exhibiting an OD of 2.50. ED@Co_3O_4NPs showed hemolysis activity at concentrations from 0.5 to 5 μg/mL, with % hemolysis ranging from 0.10% to 3.76%. This indicates a concentration-dependent increase in the hemolytic activity of ED@Co_3O_4NPs as shown in Table 3. Since 5% hemolysis is generally regarded as the permissible limit for biomaterials, this threshold was met at concentrations up to 5.0 μg/μL of Co_3O_4NPs [74]. The observed hemolytic profile provides important insights into the biocompatibility of ED@Co_3O_4NPs. The low hemolytic activity at lower concentrations suggests that these NPs are relatively safe for biomedical applications involving lower doses. However, the marked increase in hemolytic activity at higher concentrations indicates a threat to red blood cell damage, which must be carefully considered in clinical applications. The concentration-dependent hemolytic profile highlights the necessity for thorough dose-dependent evaluations to ensure the safe and effective use of ED@Co_3O_4NPs in medical treatments and diagnostics, particularly in scenarios where NPs may come into direct contact with blood. Our results are in good agreement with the previous literature on the Co_3O_4NP hemolytic activity [31].

3.12 | Anticoagulant and Thrombolytic Analysis of ED@Co_3O_4NPs

The anticoagulant activity of biosynthesized ED@Co_3O_4NPs was assessed by treating human blood samples with varying concentrations of NPs and monitoring coagulation over time. Figure 9 shows four test tubes labeled A, B, C, and D, each containing different amounts of ED@Co_3O_4NPs. In the control sample (Tube A, without ED@Co_3O_4NPs), coagulation began

TABLE 4 | Comparative biological performance of green and nongreen synthesized Co_3O_4NPs.

Synthesis method	Reducing/stabilizing source	Characterization reported	Antibacterial activity (zone of inhibition/MIC)	Other biological activities	Remarks	Ref
Green synthesis (plant-mediated)	*E. diffusum* extract	UV–Vis, FTIR, SEM, XRD, EDX, DLS, Zeta potential, TGA/DSC	25 mm (*P. aeruginosa*), 22 mm (*E. coli*), 12 mm (*S. epidermidis*)	Antioxidant (DPPH 80.41%), FRAP (70.44 mg·AAE/g), hemolysis (< 5%), anticoagulant, thrombolytic	Broad-spectrum bioactivity + eco-friendly synthesis	This study
Chemical coprecipitation	NaOH-based precipitation	SEM, XRD, FTIR	8–10 mm (*E. coli*, *S. aureus*)	Antibacterial only	Chemical route; lower inhibition compared to green route	[18]
Green plant–mediated	Phytolacca dodecandra extract	SEM, XRD, FTIR	10–12 mm (*E. coli*, *S. aureus*)	Antibacterial only	Moderate activity	[76]
Green synthesis	Plant extract	SEM, XRD, FTIR	MIC 23–26 μg/mL	Antifungal, Larvicidal	Quantitative MIC data reported	[77]
Nongreen electrosynthesis	Chemical method + annealing	HRSEM, XRD, BET	Variable inhibition (dependent on temperature)	Antifungal	Activity dependent on processing temperature	[78]

within 15 min of incubation. The blood sample thickened over time, forming a large clot after 60 min. In Tube B, with 20 μg/mL of Co_3O_4NPs, the blood sample also coagulated within 60 min. However, in Tube C, which contained 30 μg/mL of ED@Co_3O_4NPs, there were no significant changes observed in the blood sample after 60 min of incubation, indicating the onset of anticoagulant activity. Tube D, with 40 μg/mL of ED@Co_3O_4NPs, showed the best anticoagulant activity, as no signs of coagulation were found even after 60 min of incubation. This observation is in line with previous publications on the thrombolytic behavior of Co_3O_4NPs mediated by red algae, but there are limited data available in the literature on the use of nano-cobalt as an anticoagulant and thrombolytic agent [22]. These results were consistent with those of earlier studies on the anticoagulant effects of silver NPs [32, 75].

The thrombolytic activity of biogenic ED@Co_3O_4NPs was evaluated by applying different volumes (10, 20, 30, and 40 μL) of the NP suspension to preformed blood clots on the slides. Blood clots were allowed to interact with the NPs for 30 min. In Figure 10(a), the blood clots remained intact on the slides, labeled a, b, c, and d, each corresponding to a different volume of ED@Co_3O_4NPs to be applied. After 30 min (Figure 10(b)), the clot on slide "a" (10 μg/mL of ED@Co_3O_4NPs) showed partial liquefaction. The clot on slide "b" (20 μg/mL) exhibited further dissolution, and the clot on slide "c" (30 μg/mL) showed significant liquefaction. Notably, the clot on slide "d" (40 μg/mL) was completely dissolved, indicating that 40 μg/mL of ED@Co_3O_4NPs is the most effective volume for achieving complete clot dissolution within the observed time frame. These results confirm the potent thrombolytic activity of ED@Co_3O_4NPs, with the highest concentration (40 μg/mL) demonstrating the ability to completely dissolve blood clots within 30 min. Although the present study provides visual and qualitative evidence of anticoagulant and thrombolytic activity, future investigations will incorporate quantitative analyses, including clot weight reduction percentage, spectrophotometric clot lysis measurement, plasma recalcification time (PRT), prothrombin time (PT), and activated partial thromboplastin time (aPTT), to provide a more comprehensive and mechanistic evaluation of ED@Co_3O_4NPs in hemostatic modulation.

3.13 | Comparison With Previous Literature

The comparison analysis shows that the biosynthesized ED@Co_3O_4NPs show competitive and in some cases even better antibacterial performance as illustrated in Table 4. Many of the other nongreen synthetic methodologies depend on the use of chemical reducing agents, extensive heat treatment or surfactants, that can lead to residual toxicity and may impede their biomedical applications. On the other hand, plant-mediated synthesis applied in this work uses *E. diffusum* extract as a natural reducing and stabilizing agent without employing toxic chemicals, which makes it possible to produce promising green fabrication protocol.

Moreover, most of the previously investigated studies have only concentrated on antibacterial evaluation; however, this study offers an extensive biological evaluation including antioxidant, hemolytic anticoagulant, and thrombolytic assays. This comprehensive evaluation strengthens the biomedical relevance of the synthesized NPs beyond simple antimicrobial screening. The

significant inhibition zones against *P. aeruginosa* and *E. coli* and good hemocompatibility results indicate that phytochemical-based surface modification could help with improved biological interactions.

The combined adoption of green synthesis, detailed physicochemical analysis, and versatile biological evaluation demonstrates the potential benefits of plant-mediated route for ecofriendly cytocompatible, biodegradable Co_3O_4NPs suitable for advanced biomedical applications.

4 | Conclusion

The present study successfully synthesized Co_3O_4NPs using *E. diffusum* aqueous extract, establishing an eco-friendly, cost-effective, and efficient green synthesis route. The characterization of ED@Co_3O_4NPs confirmed their nanoscale size, with UV–Vis spectroscopy showing an absorption peak at 323 nm, FTIR analysis revealing functional groups responsible for NP stabilization, SEM indicating a uniform spherical morphology with an average diameter of 58.56 nm, XRD confirming the crystalline structure with an average crystallite size of approximately 15.17 nm, and EDX analysis showing the elemental composition of the NPs. DLS and zeta potential analyses further confirmed the stability and size distribution of the synthesized NPs. The greenly synthesized ED@Co_3O_4NPs exhibited significant antibacterial activity, particularly against *P. aeruginosa* and *E. coli*, with zones of inhibition measuring 25 mm and 22 mm, respectively. The antioxidant activity, assessed through DPPH and FRAP assays, showed a concentration-dependent increase in scavenging activity, with DPPH scavenging percentages rising from 38.75% at 100 to 80.4 1% at 300 μL and FRAP reducing power increasing from 26.05 at 100 to 70.44 mg AAE/g at 300 μL. Hemolytic studies confirmed biocompatibility at lower concentrations (% hemolysis = 0.10%–3.76%). NPs also demonstrated excellent anticoagulant and thrombolytic properties, with significant inhibition of blood coagulation and complete dissolution of blood clots at higher concentrations. The green synthesized ED@Co_3O_4NPs show promising potential for various biomedical applications, including antibacterial, antioxidant, anticoagulant, and thrombolytic activities.

Author Contributions

Conceptualized and study designed: Muhammad Naeem-ul-Hassan, Muhammad Fayyaz Ur Rehman, and Nasir Assad. Data curation: Nasir Assad, Tehreem Riaz, and Iram Zahra Writing original draft preparation: Nasir Assad, Marzia Batool Laila, and Ahmed Vandy. Writing–review and editing: Muhammad Nauman Khan, Sharia Fatima, Ahmed Vandy, and Barkat Ullah. Supervision: Muhammad Naeem-ul-Hassan and Muhammad Fayyaz Ur Rehman.

Acknowledgments

The authors extend their sincere gratitude to mentors, colleagues, and peers whose guidance and encouragement were invaluable throughout this research journey. Special appreciation is given to the Higher Education Commission (HEC) Pakistan for academic support through the Indigenous Scholarship program (Project No. 520-161352-2PS6-111(50093302)), which provided the opportunity to pursue advanced study and scholarly growth.

Funding

No funding was received for this research.

Disclosure

All authors critically reviewed and approved the final version.

Ethics Statement

The study was approved by the Biosafety and Ethical Review Committee ORIC, University of Sargodha, Pakistan (Ref no: SU/ORIC/2073). The *E. diffusum* D plants were collected from Tehsil Mir Ali, District North Waziristan, Khyber Pakhtunkhwa. The plant sample (*E. diffusum D*) was collected from a privately owned land belonging to one of the authors, located in North Waziristan, Khyber Pakhtunkhwa, Pakistan, where the species grows naturally. The species is wild, not protected, and not listed as endangered. Therefore, no specific permissions or licenses were required for its collection. All procedures complied with relevant institutional, national, and international guidelines and legislation.

Consent

All participants provided written informed consent prior to their inclusion in the study, and all procedures were conducted in accordance with relevant ethical standards.

Conflicts of Interest

The authors declare no conflicts of interest.

Data Availability Statement

The data that support the findings of this study are available from the corresponding author upon reasonable request.

References

1. Y. Rowhani, S. Reiisi, and M. Feizi-Dehnayebi, "Eugenol-Loaded Zinc Oxide Nanoparticles Enhance Paclitaxel Sensitivity in Breast Cancer Cells: A Combined Synergistic Nanomedicine and Theoretical Approach," *Results in Chemistry* 19 (2025): 102941, https://doi.org/10.1016/j.rechem.2025.102941.

2. S. Malik, K. Muhammad, and Y. Waheed, "Nanotechnology: A Revolution in Modern Industry," *Molecules* 28, no. 2 (2023): 661, https://doi.org/10.3390/molecules28020661.

3. N. Assad, A. Abbas, M. F. ur Rehman, and M. Naeem-ul-Hassan, "Photo-Catalytic and Biological Applications of Phyto-Functionalized Zinc Oxide Nanoparticles Synthesized Using a Polar Extract of *Equisetum diffusum* D," *RSC Advances* 14, no. 31 (2024): 22344–22358, https://doi.org/10.1039/d4ra03573a.

4. A. Jabbar, A. Abbas, N. Assad, et al., "A Highly Selective Hg 2+ Colorimetric Sensor and Antimicrobial Agent Based on Green Synthesized Silver Nanoparticles Using *Equisetum diffusum* Extract," *RSC Advances* 13, no. 41 (2023): 28666–28675, https://doi.org/10.1039/d3ra05070j.

5. S. S. Hashmi, M. Ibrahim, M. Adnan, et al., "Green Synthesis of Silver Nanoparticles From *Olea europaea* L. Extracted Polysaccharides, Characterization, and Its Assessment as an Antimicrobial Agent Against Multiple Pathogenic Microbes," *Open Chemistry* 22, no. 1 (2024): 20240016, https://doi.org/10.1515/chem-2024-0016.

6. N. George and D. G. Devi, "Phytonano Silver for Cosmetic Formulation-Synthesis, Characterization, and Assessment of Antimicrobial and Antityrosinase Potential," *Discover Nano* 19, no. 1 (2024): 65, https://doi.org/10.1186/s11671-024-04008-6.

7. A. I. Osman, Y. Zhang, M. Farghali, et al., "Synthesis of Green Nanoparticles for Energy, Biomedical, Environmental, Agricultural, and Food Applications: a Review," *Environmental Chemistry Letters* 22, no. 2 (2024): 841–887, https://doi.org/10.1007/s10311-023-01682-3.

8. Z. U. R. Khan, N. Assad, M. Naeem-ul-Hassan, et al., "*Aconitum lycoctonum* L. (Ranunculaceae) Mediated Biogenic Synthesis of Silver Nanoparticles as Potential Antioxidant, Anti-Inflammatory, Antimicrobial and Antidiabetic Agents," *BMC Chemistry* 17, no. 1 (2023): 128, https://doi.org/10.1186/s13065-023-01047-5.

9. G. M. Ziarani, S. Shaabani, Z. Panahande, A. Badiei, and M. Feizi-Dehnayebi, "Fluorescent Nanosensor Based on Fumed-Silica Modified With Terephthalaldehyde and Indandione for Selective Hg2+ Detection: DFT and Experimental Viewpoints," *Journal of Molecular Structure* 1359 (2026): 145348, https://doi.org/10.1016/j.molstruc.2026.145348.

10. R. Shanmuganathan, S. Sathiyavimal, Q. Hoang Le, et al., "Green Synthesized Cobalt Oxide Nanoparticles Using Curcuma Longa for Anti-Oxidant, Antimicrobial, Dye Degradation and Anti-Cancer Property," *Environmental Research* 236 (2023): 116747, https://doi.org/10.1016/j.envres.2023.116747.

11. S. Ullah, et al., "Phytomediated Selenium Doped Au/ZnO/Fe_3O_4 Nanocomposites for Synergistic Photocatalytic Dye Degradation and Mercury (II) Detection," *Scientific Reports* (2025): https://www.nature.com/articles/s41598-025-30833-5.

12. N. E. Eleraky, A. Allam, S. B. Hassan, and M. M. Omar, "Nanomedicine Fight Against Antibacterial Resistance: An Overview of the Recent Pharmaceutical Innovations," *Pharmaceutics* 12, no. 2 (2020): 142, https://doi.org/10.3390/pharmaceutics12020142.

13. Tooba, N. Assad, M. B. Laila, et al., "Green Synthesis of Silver Nanoparticles Using *Solanum lycopersicum* Leaves Extract for Highly Selective Detection of Mercury Ions and Photocatalytic Degradation of Methylene Blue," *Discover Nano* 21, no. 1 (2026): 14, https://doi.org/10.1186/s11671-025-04424-2.

14. A. Noor, N. Ahmad, A. Ali, et al., "Green Synthesis of Silver-Doped ZnO Nanoparticles From *Adiantum venustum* D. Don (Pteridaceae): Antimicrobial and Antioxidant Evaluation," *Journal of Basic Microbiology* 65, no. 4 (2025): e2400543, https://doi.org/10.1002/jobm.202400543.

15. N. Assad, M. Naeem-ul-Hassan, M. Ajaz Hussain, et al., "Diffused Sunlight Assisted Green Synthesis of Silver Nanoparticles Using *Cotoneaster nummularia* Polar Extract for Antimicrobial and Wound Healing Applications," *Natural Product Research* 39, no. 8 (2023): 1–15, https://doi.org/10.1080/14786419.2023.2295936.

16. N. Riaz, F. Zubair, A. Ali, et al., "Plant Based Antimicrobials Against Multi Drug Resistant Bacterial Strains (MDRS)," *Polish Journal of Environmental Studies* 34, no. 4 (2025): 4799–4806, https://doi.org/10.15244/pjoes/190564.

17. E. Boluki, M. Pourhajibagher, and A. Bahador, "The Combination of Antimicrobial Photocatalysis and Antimicrobial Photodynamic Therapy to Eradicate the Extensively Drug-Resistant Colistin Resistant Acinetobacter baumannii," *Photodiagnosis and Photodynamic Therapy* 31 (2020): 101816, https://doi.org/10.1016/j.pdpdt.2020.101816.

18. F. K. Sabir, E. T. Bekele, B. A. Gonfa, G. D. Edossa, and A. T. Adino, "Synthesis of Cobalt Oxide Nanoparticles Through Chemical and Biological Pathways for Antibacterial Activity," *Journal of Nanostructures* 11 (2021): 577–587.

19. K. U. Suganya, K. Govindaraju, V. Ganesh Kumar, et al., "Blue Green Alga Mediated Synthesis of Gold Nanoparticles and Its Antibacterial Efficacy Against Gram Positive Organisms," *Materials Science and Engineering: C* 47 (2015): 351–356, https://doi.org/10.1016/j.msec.2014.11.043.

20. S. Haq, F. Abbasi, M. Ben Ali, et al., "Green Synthesis of Cobalt Oxide Nanoparticles and the Effect of Annealing Temperature on Their Physiochemical and Biological Properties," *Materials Research Express* 8, no. 7 (2021): 075009, https://doi.org/10.1088/2053-1591/ac1187.

21. A. Safdar, H. E. A. Mohamed, K. Hkiri, A. Muhaymin, and M. Maaza, "Green Synthesis of Cobalt Oxide Nanoparticles Using Hyphaene thebaica Fruit Extract and Their Photocatalytic Application," *Applied Sciences* 13, no. 16 (2023): 9082, https://doi.org/10.3390/app13169082.

22. J. S. Ajarem, S. N. Maodaa, A. A. Allam, M. M. Taher, and M. Khalaf, "Benign Synthesis of Cobalt Oxide Nanoparticles Containing Red Algae Extract: Antioxidant, Antimicrobial, Anticancer, and Anticoagulant Activity," *Journal of Cluster Science* 33, no. 2 (2021): 1–12, https://doi.org/10.1007/s10876-021-02004-9.

23. M. A. Mir, M. W. Ashraf, and B. A. Mir, "Antimicrobial and Antifungal and Phytochemical Analysis of Various Extracts of *Equisetum diffusum*," *Phytochemical Analysis* 11 (2021): 13.

24. T. Das, P. Holland, M. Ahmed, and L. Husain, "Sustainable Development Goal 3: Good Health and Well-Being," in *South-East Asia Eye Health*, ed. T. Das and P. D. Nayar (Singapore: Springer Singapore, 2021), 61–78, https://doi.org/10.1007/978-981-16-3787-2_4.

25. I. B. Franco and L. Newey, "SDG 12 Responsible Consumption and Production: Sustainable Community Development Through Entrepreneurship: Corporate-Based Versus Wellbeing-Centred Approaches to Responsible Production," in *Actioning the Global Goals for Local Impact*, ed. I. B. Franco, T. Chatterji, E. Derbyshire, and J. Tracey (Singapore: Springer Singapore, 2020), 187–217, https://doi.org/10.1007/978-981-32-9927-6_13.

26. G. M. Ziarani, A. Arvish, Z. Panahande, A. Badiei, and M. Feizi-Dehnayebi, "Enhancing Sensor Performance Through the Surface Functionalization of SBA-15 With 2-Chloroquinoline-3-Carbaldehyde and Sulphaguanidine Verified via DFT Insights," *Chemical Engineering Journal Advances* 24 (2025): 100923, https://doi.org/10.1016/j.ceja.2025.100923.

27. T. Roheen, M. Bibi, M. Fu Rehman, et al., "Enhanced Antibacterial and Anti-Inflammatory Efficiency of Serratiopeptidase Immobilized on CMC-Silver Nanoparticles," *Journal of Basic Microbiology* 65, no. 11 (2025): e70060, https://doi.org/10.1002/jobm.70060.

28. N. Assad, M. B. Laila, M. N. U. Hassan, et al., "Eco-Friendly Synthesis of Gold Nanoparticles Using *Equisetum diffusum* D. Don. With Broad-Spectrum Antibacterial, Anticancer, Antidiabetic, and Antioxidant Potentials," *Scientific Reports* 15, no. 1 (2025): 19246, https://doi.org/10.1038/s41598-025-02450-9.

29. H. Gula, et al., "Exploring the Antibacterial, Anticoagulant, and Hemolytic Potential of Green-Synthesized Fe 2 O 3 Nanoparticles by Cucurbita Pepo Pulp," *IEEE Transactions on NanoBioscience* (2025): https://ieeexplore.ieee.org/abstract/document/10973190/.

30. K. Demirgül and E. Ozturk, "Changes in Nutrients, Energy, Antioxidant and Carotenoid Levels of Dried Tomato (*Lycopersicon esculentum*) Pomage Treated With Aspergillus Niger Solid-State Fermentation," *Turkish Journal of Agriculture-Food Science and Technology* 9, no. 4 (2021): 701–708, https://doi.org/10.24925/turjaf.v9i4.701-708.4014.

31. D. Das and B. J. Saikia, "Synthesis, Characterization and Biological Applications of Cobalt Oxide (Co3O4) Nanoparticles," *Chemical Physics Impact* 6 (2023): 100137, https://doi.org/10.1016/j.chphi.2022.100137.

32. M. A. Azeez, F. A. Durodola, A. Lateef, et al., "Green Synthesized Novel Silver Nanoparticles and Their Application as Anticoagulant and Thrombolytic Agents: A Perspective," in *IOP Conference Series: Materials Science and Engineering*, 805, no. 1 (IOP Publishing, 2020), 012043, https://doi.org/10.1088/1757-899x/805/1/012043.

33. S. Kumar, A. Kaur, J. Gaur, et al., "State-of-the-Art in Co_3O_4 Nanoparticle Synthesis and Applications: Toward a Sustainable Future," *ChemistrySelect* 10, no. 6 (2025): e202405147, https://doi.org/10.1002/slct.202405147.

34. N. Devi, K. Kumar, A. Kumar, and N. Thakur, "Catalytic Properties of *Thuja occidentalis* Green Synthesized Yb Doped MgFe2O4, CuFe2O4 and MgCuFe2O4 Ferrite Nanoparticles," *Nano-Structures & Nano-Objects* 44 (2025): 101554, https://doi.org/10.1016/j.nanoso.2025.101554.

35. H. R. Ghorbani, F. P. Mehr, and A. K. Poor, "Extracellular Synthesis of Copper Nanoparticles Using Culture Supernatants of *Salmonella typhimurium*," *Oriental Journal of Chemistry* 31, no. 1 (2015): 527–529, https://doi.org/10.13005/ojc/310165.

36. A. Waris, M. Din, A. Ali, et al., "Green Fabrication of Co and Co_3O_4 Nanoparticles and Their Biomedical Applications: A Review," *Open Life Sciences* 16, no. 1 (2021): 14–30, https://doi.org/10.1515/biol-2021-0003.

37. I. Bibi, N. Nazar, M. Iqbal, et al., "Green and Eco-Friendly Synthesis Of Cobalt-Oxide Nanoparticle: Characterization and Photo-Catalytic Activity," *Advanced Powder Technology* 28, no. 9 (2017): 2035–2043, https://doi.org/10.1016/j.apt.2017.05.008.

38. I. Lisiecki and M. P. Pileni, "Synthesis of Well-Defined and Low Size Distribution Cobalt Nanocrystals: The Limited Influence of Reverse Micelles," *Langmuir* 19, no. 22 (2003): 9486–9489, https://doi.org/10.1021/la0301386.

39. G. A. Kahrilas, L. M. Wally, S. J. Fredrick, M. Hiskey, A. L. Prieto, and J. E. Owens, "Microwave-Assisted Green Synthesis of Silver Nanoparticles Using Orange Peel Extract," *ACS Sustainable Chemistry and Engineering* 2, no. 3 (2014): 367–376, https://doi.org/10.1021/sc4003664.

40. T. Rasheed, F. Nabeel, M. Bilal, and H. M. Iqbal, "Biogenic Synthesis and Characterization of Cobalt Oxide Nanoparticles for Catalytic Reduction of Direct Yellow-142 and Methyl Orange Dyes," *Biocatalysis and Agricultural Biotechnology* 19 (2019): 101154, https://doi.org/10.1016/j.bcab.2019.101154.

41. M. R. Pallavolu, K. G. Krishna, G. Nagaraju, P. S. Babu, S. Sambasivam, and A. Sreedhar, "Rational Design of Cu-Doped Co3O4@Carbon Nanocomposite and Agriculture Crop-Waste Derived Activated Carbon for High-Performance Hybrid Supercapacitors," *Journal of Industrial and Engineering Chemistry* 116 (2022): 428–437, https://doi.org/10.1016/j.jiec.2022.09.033.

42. Ravina, G. Srivastava, S. Dalela, et al., "Study of Structural, Optical, Surface and Electrochemical Properties of Co3O4 Nanoparticles for Energy Storage Applications," *Interactions* 245, no. 1 (2024): 85, https://doi.org/10.1007/s10751-024-01932-y.

43. S. Ghaffar, A. Abbas, M. Naeem-ul-Hassan, et al., "Improved Photocatalytic and Antioxidant Activity of Olive Fruit Extract-Mediated ZnO Nanoparticles," *Antioxidants* 12, no. 6 (2023): 1201, https://doi.org/10.3390/antiox12061201.

44. M. Alzaid, A. M. Abu-Dief, N. M. A. Hadia, M. Ezzeldien, and W. S. Mohamed, "Synthesis and Characterization Study of Spinel Co3O4 Nanoparticles Synthesized via the Facial Co-Precipitation Route for Optoelectronic Application," *Optical and Quantum Electronics* 56, no. 7 (2024): 1156, https://doi.org/10.1007/s11082-024-07095-y.

45. A. Puspalak, P. Chinnadurai, R. Prathibha, et al., "Cobalt Oxide Nanoparticles Based Carbon Electrode for the Detection of Residual Nitrite in the Soil of Agricultural Fields," *Materials Research Innovations* 27, no. 2 (2023): 100–109, https://doi.org/10.1080/14328917.2022.2085909.

46. S. Savitha, S. Surendhiran, K. S. G. Jagan, A. Karthik, B. Kalpana, and R. Senthilmurugan, "Evaluation of the Physicochemical Characteristics and Photocatalytic Activity of Cobalt Oxide Nanoparticles Derived From Moringa Seed Extract," *Journal of Materials Science: Materials in Electronics* 34, no. 2 (2023): 89, https://doi.org/10.1007/s10854-022-09506-w.

47. P. Chelliah, S. M. Wabaidur, H. P. Sharma, et al., "Green Synthesis and Characterizations of Cobalt Oxide Nanoparticles and Their Coherent Photocatalytic and Antibacterial Investigations," *Water* 15, no. 5 (2023): 910, https://doi.org/10.3390/w15050910.

48. C.-W. Tang, C.-B. Wang, and S.-H. Chien, "Characterization of Cobalt Oxides Studied by FT-IR, Raman, TPR and TG-MS," *Thermochimica Acta* 473, no. 1-2 (2008): 68–73, https://doi.org/10.1016/j.tca.2008.04.015.

49. A. Bahadoran, S. Ramakrishna, B. Oryani, L. Ahmed Al-Keridis, H. Rashidi Nodeh, and S. Rezania, "Biodiesel Production From Waste Cooking Oil Using Heterogeneous Nanocatalyst-Based Magnetic Polyaniline Decorated With Cobalt Oxide," *Fuel* 319 (2022): 123858, https://doi.org/10.1016/j.fuel.2022.123858.

50. A. K. Singh, "A Review on Plant Extract-Based Route for Synthesis of Cobalt Nanoparticles: Photocatalytic, Electrochemical Sensing and Antibacterial Applications," *Current Research in Green and Sustainable Chemistry* 5 (2022): 100270, https://doi.org/10.1016/j.crgsc.2022.100270.

51. S. Gopinath, M. Mayakannan, and S. Vetrivel, "Analysis on the Effect of Doping in Structural, Morphological, and Antibacterial Properties of Yttrium Doped Cobalt Oxide Nanoparticles," *Materials Technology* 37, no. 13 (2022): 2425–2435, https://doi.org/10.1080/10667857.2022.2038765.

52. V. Raman, S. Suresh, P. A. Savarimuthu, et al., "Synthesis of Co3O4 Nanoparticles With Block and Sphere Morphology, and Investigation Into the Influence of Morphology on Biological Toxicity," *Experimental and Therapeutic Medicine* 11, no. 2 (2016): 553–560, https://doi.org/10.3892/etm.2015.2946.

53. N. Al-Qasmi, "Sustainable and Efficacy Approach of Green Synthesized Cobalt Oxide (Co3O4) Nanoparticles and Evaluation of Their Cytotoxicity Activity on Cancerous Cells," *Molecules* 27, no. 23 (2022): 8163, https://doi.org/10.3390/molecules27238163.

54. A. Imtiyaz, A. Singh, and R. Gaur, "Comparative Analysis and Applications of Green Synthesized Cobalt Oxide (Co3O4) Nanoparticles: A Systematic Review," *BioNanoScience* 1–19 (2024).

55. S. Chaturvedi, D. Maheshwari, A. Chawathe, and N. Sharma, "Current Analytical Approaches for Characterizing Nanoparticle Sizes in Pharmaceutical Research," *Journal of Nano Research* 26, no. 1 (2024): 19, https://doi.org/10.1007/s11051-023-05924-x.

56. P. J. Jalil, R. M. Mhamedsharif, B. H. Shnawa, S. M. Hamad, P. Aspoukeh, and M. H. Ahmed, "Comparative Assessment of Anti-Inflammatory and Catalytic Properties of Chemically Synthesised and Green-Synthesised Silver Nanoparticles From *Ziziphus spina-christi* Leaf Extract," *Toxicology and Environmental Health Sciences* 17, no. 1 (2025): 95–113, https://doi.org/10.1007/s13530-025-00252-0.

57. M. Mehrafza, S. Daneshjou, K. Khajeh, and A. A. Sepahi, "Green Fabrication of Cobalt Oxide Nanoparticles by *Bacillus megaterium* and Their Antibacterial Activities," *BioNanoScience* 1–12 (2024).

58. D. Sharma, P. Shandilya, N. Saini, et al., "Insights Into the Synthesis and Mechanism of Green Synthesized Antimicrobial Nanoparticles, Answer to the Multidrug Resistance," *Materials Today Chemistry* 19 (2021): 100391, https://doi.org/10.1016/j.mtchem.2020.100391.

59. M. Sharma, Monika, P. Thakur, R. V. Saini, R. Kumar, and E. Torino, "Unveiling Antimicrobial and Anticancerous Behavior of AuNPs and AgNPs Moderated by Rhizome Extracts of *Curcuma longa* From Diverse Altitudes of Himalaya," *Scientific Reports* 10, no. 1 (2020): 10934, https://doi.org/10.1038/s41598-020-67673-4.

60. N. S. Wigginton, K. L. Haus, and Jr, M. F. Hochella, "Aquatic Environmental Nanoparticles," *Journal of Environmental Monitoring* 9, no. 12 (2007): 1306–1316, https://doi.org/10.1039/b712709j.

61. M. Alavi and M. Rai, "Recent Advances in Antibacterial Applications of Metal Nanoparticles (MNPs) and Metal Nanocomposites (MNCs) Against Multidrug-Resistant (MDR) Bacteria," *Expert Review of Anti-infective Therapy* 17, no. 6 (2019): 419–428, https://doi.org/10.1080/14787210.2019.1614914.

62. A. Singh, P. K. Gautam, A. Verma, et al., "Green Synthesis of Metallic Nanoparticles as Effective Alternatives to Treat Antibiotics Resistant Bacterial Infections: A Review," *Biotechnology Reports* 25 (2020): e00427, https://doi.org/10.1016/j.btre.2020.e00427.

63. N. Assad, et al., "Green Synthesis of Selenium Nanoparticles Using *Equisetum diffusum*: Characterization, Antibacterial Potential, Effects on Plant Growth," *IEEE Transactions on NanoBioscience* (2025): https://ieeexplore.ieee.org/abstract/document/10988879/.

64. P. K. Stoimenov, R. L. Klinger, G. L. Marchin, and K. J. Klabunde, "Metal Oxide Nanoparticles as Bactericidal Agents," *Langmuir* 18, no. 17 (2002): 6679–6686, https://doi.org/10.1021/la0202374.

65. A. Thill, O. Zeyons, O. Spalla, et al., "Cytotoxicity of CeO_2 Nanoparticles for *Escherichia coli*. Physico-Chemical Insight of the Cytotoxicity Mechanism," *Environmental Science & Technology* 40, no. 19 (2006): 6151–6156, https://doi.org/10.1021/es060999b.

66. Y. N. Slavin, J. Asnis, U. O. Häfeli, and H. Bach, "Metal Nanoparticles: Understanding the Mechanisms Behind Antibacterial Activity," *Journal of Nanobiotechnology* 15, no. 1 (2017): 65, https://doi.org/10.1186/s12951-017-0308-z.

67. Y. Bibi, Z. Nasreen, H. Gul, et al., "Phytosynthesis of Gold Nanoparticles From *Boerhavia diffusa* L. and Their Antibacterial, Antifungal, Antioxidant, and Anticancer Activities," *Discover Nano* 21, no. 1 (2026): 7, https://doi.org/10.1186/s11671-025-04425-1.

68. T. Roheen, et al., "Improved Destaining and Antimicrobial Potential of Pepsin Cross-linked HPMC-Se Nanoparticles," *IEEE Transactions on Nano-Bioscience* (2025): https://ieeexplore.ieee.org/abstract/document/11316155/.

69. A. Simon-Deckers, S. Loo, M. Mayne-L'hermite, et al., "Size-Composition- and Shape-Dependent Toxicological Impact of Metal Oxide Nanoparticles and Carbon Nanotubes Toward Bacteria," *Environmental Science & Technology* 43, no. 21 (2009): 8423–8429, https://doi.org/10.1021/es9016975.

70. F. Farzandi, G. M. Ziarani, S. Reiisi, A. Badiei, and M. Feizi-Dehnayebi, "Tetrazole-Based Fluorescent Probe for Sensitive Detection of Cu2+: Photoluminescence, Biological Activity, DNA/BSA Interaction, and Theoretical Insights," *Results in Chemistry* (2025): 102992.

71. S. B. Hussain, S. Zahra, S. Hussain, et al., "Characterization and Comparative Antibacterial Activities of Gold Nanoparticles Synthesized by *Tagetes patula* L. (Asteraceae) Flower Extract," *Microscopy Research and Technique* 88, no. 6 (2025): 1869–1880, https://doi.org/10.1002/jemt.24829.

72. A. Prakash, S. Sur, V. Dave, et al., "Green Synthesized Cobalt Nanoparticles From *Trianthema portulacastrum* L. as a Novel Antimicrobials and Antioxidants," *Preparative Biochemistry & Biotechnology* (2023): 1–15, https://doi.org/10.1080/10826068.2023.2238306.

73. M. Feizi-Dehnayebi, G. Mohammadi Ziarani, S. Reiisi, et al., "Biological Evaluations and Biomolecular Interactions Along With Computational Insights of Arylidene Isatin Hydrazones Synthesized Using Nanocatalyst," *Scientific Reports* 15, no. 1 (2025): 42705, https://doi.org/10.1038/s41598-025-26721-7.

74. J. P. Singhal and A. R. Ray, "Synthesis of Blood Compatible Polyamide Block Copolymers," *Biomaterials* 23, no. 4 (2002): 1139–1145, https://doi.org/10.1016/s0142-9612(01)00228-9.

75. D. A. Aina, O. Owolo, A. Lateef, et al., "Biomedical Applications of Chasmanthera dependens Stem Extract Mediated Silver Nanoparticles as Antimicrobial, Antioxidant, Anticoagulant, Thrombolytic, and Larvicidal Agents," *Karbala International Journal of Modern Science* 5 (2019): 2, https://doi.org/10.33640/2405-609x.1018.

76. N. Akhter, A. Liaquat, F. Murtaza, et al., "One-Step Phytosynthesis of Co3O4 Nanoparticles and Study of Their Catalytic, Antioxidant, Antibiofilm and Antibacterial Activities," *Results in Chemistry* 14 (2025): 102151, https://doi.org/10.1016/j.rechem.2025.102151.

77. P. Gowthami, A. Kosiha, S. Meenakshi, G. Boopathy, A. G. Ramu, and D. Choi, "Biosynthesis of Co3O4 Nanomedicine by Using *Mollugo oppositifolia* L. Aqueous Leaf Extract and Its Antimicrobial, Mosquito Larvicidal Activities," *Scientific Reports* 13, no. 1 (2023): 9002, https://doi.org/10.1038/s41598-023-35877-z.

78. I. M. Omar, M. E. Sayed, M. A. Ibrahim, and M. A. El-Jemni, "Electrosynthesis and Phase Control of Cobalt-Based Nanoparticles: Antibacterial and Antifungal Evaluation of CO_3O_4 Formed at Varied Temperatures," *Chemistry* 7, no. 3 (2025): 87, https://doi.org/10.3390/chemistry7030087.